Available online at www.sciencedirect.com
ScienceDirect
International Journal of Heat and Mass Transfer 51 (2008) 4276–4286
International Journal of HEAT and MASS TRANSFER
www.elsevier.com/locate/ijhmt

# Turbulent mixing of a passive scalar in confined multiple jet flows of a micro combustor

Hang Seok Choi [a,*], Tae Seon Park [b], Kenjiro Suzuki [c,✠]

[a] Environmental Systems Research Center, Environment and Energy Research Division, Korea Institute of Machinery and Materials, 171 Jang-dong, Yuseong-gu, Daejeon 305-343, South Korea
[b] School of Mechanical Engineering, Kyungpook National University, 1370 Sangyeok-dong, Buk-gu, Daegu 702-701, South Korea
[c] Department of Machinery and Control Systems, Shibaura Institute of Technology, 307 Fukasaku, Saitama 337-8570, Japan

Received 11 July 2007; received in revised form 7 November 2007
Available online 3 March 2008

**Abstract**

The turbulent mixing characteristics of multiple jet flows in a micro can type combustor are investigated by means of large eddy simulation (LES). The micro combustor can be used for a micro gas turbine which is hybridized with solid oxide fuel cell. Attention is paid for a micro combustor having a circular disk baffle plate with a fuel injection nozzle in the center and oxidant injection holes allocated annularly. Downstream the baffle plate, a complex flow is produced from the interaction of multiple jet flows and study is made for three different configurations of the baffle plates resulting in different mixing pattern. From the results, it is substantiated that the turbulent mixing is promoted by complex flow fields caused by the jet flows and large vortical flow regions in the micro combustor. This is effective to accelerate the slow mixing between fuel and oxidant suffering from low Reynolds number in such a small combustor. In particular, the vortical flow region formed downstream the fuel jet core region plays an important role for rapid mixing coupled with another flow recirculation region. Discussion is made for the instantaneous and time and space averaged flow and passive scalar quantities which show peculiar turbulent flow and mixing characteristics corresponding to the different flow structures for each baffle plate shapes, respectively.


*Keywords:* Large eddy simulation; Micro combustor; Recirculation; Turbulent mixing; Vortical flow

## 1. Introduction

Currently, a micro gas turbine (MGT) has been widely drawing attention as a distributed energy generation system for an individual household or a small community. In parallel to the progress of MGT technology, a fuel cell has been highlighted for its high efficiency and environmental advantages. For MGT, its efficiency can reach to 40% [1], but it seems to be difficult to achieve higher efficiency than 40%. However, the efficiency of solid oxide fuel cell (SOFC) for electricity generation recently becomes 50% or higher [2,3]. Therefore a method hybridizing MGT with SOFC is promising technology because the MGT/SOFC hybrid system can provide higher efficiency over 70% [4]. Several concepts of the hybrid system have been suggested to elevate the system efficiency [3–5]. Among the various hybrid systems, the present study is based on the MGT/SOFC hybrid system suggested by Suzuki et al. [3]. Especially, focus is given to the turbulent mixing characteristics of a passive scalar in an innovative micro cylindrical combustor with baffle plate providing multiple fuel and oxidant jets as illustrated in Fig. 1, which is proposed as a combustor for the MGT/SOFC hybrid system by Suzuki et al. [3]. This micro combustor is expected to secure zero emission of toxic gases like CO and a stable flame for burning the effluent of SOFC in an extraordinary fuel lean condition.

Combustion in a very small chamber may not simply resemble a scaled-down version of its large-scale counter-

* Corresponding author. Tel.: +82 42 868 7398; fax: +82 42 868 7284.
*E-mail address:* hschoi@kimm.re.kr (H.S. Choi).
✠ Deceased.

0017-9310/$ - see front matter © 2008 Elsevier Ltd. All rights reserved.
doi:10.1016/j.ijheatmasstransfer.2007.12.017

**Nomenclature**

| | |
|---|---|
| CV | coefficient of variation, $CV = \frac{1}{(F_i)_{cs}} \times \sqrt{\frac{\sum_{i=1}^{n}[F_i-(F_i)_{cs}]^2}{(n-1)}}$ |
| $D$ | diffusion coefficient, $D = \nu/Sc$ |
| $D_f$ | fuel jet diameter |
| $D_o$ | oxidant jet diameter |
| $D_{tube}$ | combustor tube diameter |
| $k$ | turbulent kinetic energy, $k = \frac{1}{2}(\overline{u_i'u_i'})$ |
| $L$ | combustor length |
| $p$ | instantaneous pressure |
| $\hat{p}$ | filtered pressure |
| $\dot{Q}_i$ | total volume flow rate of species $i$ |
| $Re_{tube}$ | Reynolds number based on combustor tube diameter |
| $S_{ij}$ | strain rate tensor, $S_{ij} = (\partial u_i/\partial x_j + \partial u_j/\partial x_i)/2$ |
| $Sc$ | Schmidt number |
| $Sc_t$ | turbulent Schmidt number |
| $s_j$ | subgrid-scale scalar flux |
| $t$ | time |
| $u_i$ | instantaneous velocity |
| $U_i$ | time mean velocity |
| $u_i'$ | velocity fluctuation |
| $\hat{u}_i$ | filtered velocity |
| $\overline{u_i'u_j'}$ | Reynolds stress |
| $V_f$ | fuel jet velocity |
| $V_o$ | oxidant jet velocity |
| $f$ | instantaneous mixture fraction |
| $F$ | time mean mixture fraction |
| $(F_i)_{cs}$ | $(y,z)$ cross-sectional averaged value of $F_i$ |
| $\hat{f}$ | filtered mixture fraction |
| $f'$ | fluctuation of mixture fraction |
| $f_{rms}$ | rms of mixture fraction fluctuation, $f_{rms} = \sqrt{\overline{(f-F)^2}}$ |

*Greek symbols*

| | |
|---|---|
| $\epsilon_f$ | dissipation rate of scalar variance, $\epsilon_f = D\left(\frac{\partial f'}{\partial x_j}\right)^2 = \frac{\nu}{Sc}\left(\frac{\partial f'}{\partial x_j}\right)^2$ |
| $\Lambda_2$ | the second largest eigenvalue of $S_{ik}S_{kj} + \Omega_{ik}\Omega_{kj}$ |
| $\nu$ | kinematic molecular viscosity |
| $\rho$ | fluid density |
| $\tau_{ij}$ | subgrid-scale stress tensor |
| $\Omega_{ij}$ | vorticity tensor, $\Omega_{ij} = (\partial u_i/\partial x_j - \partial u_j/\partial x_i)/2$ |

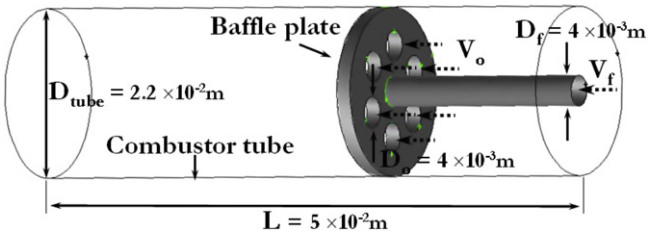


Fig. 1. Configuration of a micro can combustor for case A.

part. For example, such a small combustor may be suffering from incomplete mixing between fuel and oxidant, insufficient fuel residence time for complete combustion and high heat transfer rate to combustor outside because of high surface to volume ratio [6]. This is mainly due to the difference of geometrical dimension and Reynolds number. In the proposed micro combustor, Reynolds number based on the combustor tube diameter is very low [7–9]. Consequently, suffering from smaller residence time, mixing between fuel and oxidant is likely to become much slower, which may cause relatively longer and sooty luminous flame. In case of non-premixed combustion, to accomplish complete combustion the sum of characteristic mixing and chemical reaction time should be much smaller than residence time. Thus, the mixing enhancement is one of key factors in the development of such a small combustor satisfying another requirement to secure the flame stability. To overcome these problems, the forming of a flow recirculation region inside a combustor can be one of the solutions, which can help the scalar mixing and flame stability. However, according to Zhdanov et al. [10] if general mixing technique is used as does in a large commercial combustor, it may hard in such a small combustor to form a flow recirculation region. To solve these problems, a baffle plate with multiple jets for oxidant and fuel injections is introduced to intensify the mixing between fuel and oxidant and maintain flame stability, simultaneously. From the previous works by Choi et al. [7–9] and Woodfield et al. [11], it is seen that the proposed micro can combustor with multiple jets is very effective to meet the both requirements of mixing enhancement and flame stability.

In the present study, characteristics of turbulent flow and mixing fields in the proposed micro can combustor [3,7–9] are studied by applying the large eddy simulation (LES). Three different types of baffle plates, leading to different values of oxidant to fuel velocity ratio, are numerically tested and instantaneous and time mean quantities for the turbulent flow and mixing are scrutinized. As a result, peculiar characteristics of the turbulent mixing in the micro combustor are elucidated. Multiple recirculating flow regions appear downstream the baffle plate and these regions play an important role for the turbulent scalar mixing between oxidant jets and central fuel jet. Changing the baffle plate geometry, the shape and location of these recirculating flow regions are changed and this has a significant effect on the mixing phenomena.

## 2. Numerical methods

### 2.1. Mathematical formulation

In LES, large-scale flow and scalar quantities are defined by the convolution of the velocity, pressure and scalar fields with a filter function. General filtering operation for function $\phi(\mathbf{x},t)$ with filter function $\widehat{G}$ is defined as follows:

$$\hat{\phi}(\mathbf{x},t) = \int \widehat{G}(\mathbf{r},\mathbf{x})\phi(\mathbf{x}-\mathbf{r},t)\,\mathrm{d}\mathbf{r}. \tag{1}$$

Using the above filtering operation of turbulent quantities, filtered forms of continuity and momentum equations for incompressible fluid are reduced and they may be expressed as follows:

$$\frac{\partial \hat{u}_i}{\partial x_i} = 0, \tag{2}$$

$$\frac{\partial \hat{u}_i}{\partial t} + \hat{u}_j\frac{\partial \hat{u}_i}{\partial x_j} = \nu\frac{\partial^2 \hat{u}_i}{\partial x_j \partial x_j} - \frac{\partial \tau_{ij}}{\partial x_j} - \frac{1}{\rho}\frac{\partial \hat{p}}{\partial x_i}, \tag{3}$$

where $\hat{u}_i$, $\hat{p}$ and $\tau_{ij}$ are the filtered velocity, filtered pressure and the subgrid-scale stress tensor, respectively. In Eq. (3), $\tau_{ij}$ must be modeled. So, the dynamic subgrid-scale model [12] is adopted in the present study for $\tau_{ij}$ as follows:

$$\tau_{ij} - 1/3\delta_{ij}\tau_{kk} = -2\nu_t\widehat{S}_{ij}, \tag{4}$$

here $\nu_t$ is the eddy viscosity to be obtained.

In this article, cold mixing between fuel and oxidant is studied. The mixture fraction, $f$, is defined to be 1 for pure fuel and 0 for pure oxidant as $f = \dot{m}_{\text{fuel}}/(\dot{m}_{\text{fuel}} + \dot{m}_{\text{oxidant}})$, here $\dot{m}_i$ is the mass flux of species $i$. So, the filtered governing equation of a mixture fraction is used to represent the evolution of mixing.

$$\frac{\partial \hat{f}}{\partial t} + \frac{\partial(\hat{u}_j\hat{f})}{\partial x_j} = \frac{\partial}{\partial x_j}\left[D\left(\frac{\partial \hat{f}}{\partial x_j}\right) - s_j\right], \tag{5}$$

where $D$ is the diffusion coefficient of mixture fraction and defined as $D = \nu/Sc$. The last term of the right-hand side in Eq. (5), $s_j$, is a subgrid-scale scalar flux approximated as $s_j = -(\nu_t/Sc_t)(\partial\hat{f}/\partial x_j)$, here the value of $Sc_t$ is carefully selected according to Pitsch [13]. In the present study, the Schmidt number is set constant, i.e. $Sc = Sc_t = 0.7$.

### 2.2. Computational procedure

To numerically solve the time dependent finite-difference equivalents of Eqs. (2)–(5), a PISO (Pressure Implicit with Splitting of Operator) algorithm [14] is used. In the PISO algorithm, predictor step is discretized based on Crank–Nicolson method considering time accuracy [15,16]. As for the spatial discretization of the equations, the fourth-order COMPACT scheme [17] for the convective terms, and the fourth-order central differencing scheme for the diffusion terms and other remaining terms are applied. For the arrangement of the grids, a non-staggered grid is adopted in the generalized coordinate system. Therefore, a momentum interpolation technique is employed to avoid the pressure–velocity decoupling. The PISO algorithm used in the present study is slightly modified from Issa [14] and details regarding the solution procedure of the PISO algorithm can be found in Issa [14] and Park [15,16]. The numerical method used in the present LES is fully validated as discussed in Park [15,16] for the turbulent channel flows and for a turbulent jet flow [9].

### 2.3. Computational conditions

Figs. 1 and 2 show the computational domain and its grid system, respectively. Table 1 describes the three different calculation conditions or one condition for each baffle

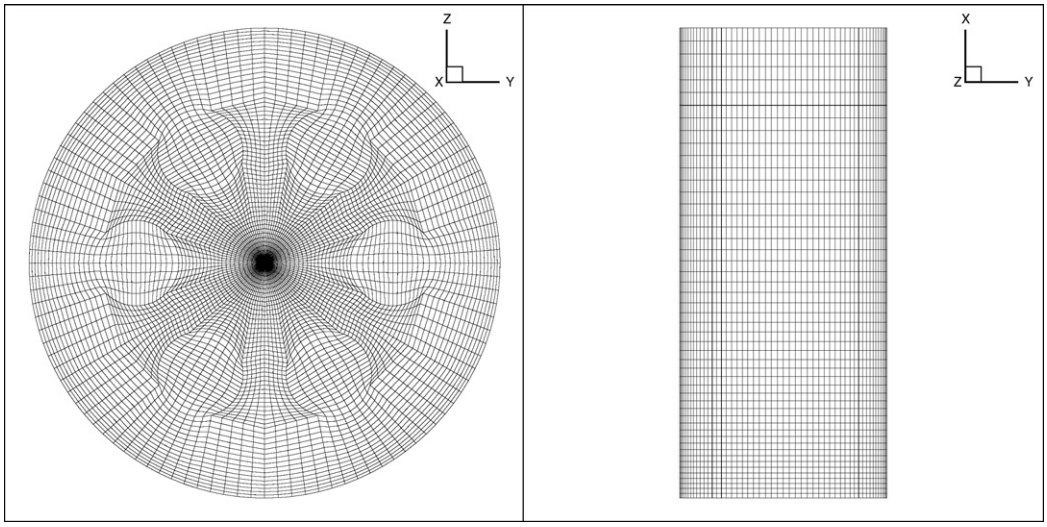


Fig. 2. Computational domain and grid system for case A.

Table 1
Calculation condition

| Case | $D_o/D_f$ | $V_o/V_f$ | $Re_{tube}$ |
|---|---|---|---|
| A | 1 | 2 | 3060 |
| B | 2 | 0.5 | 3060 |
| C | 0.5 | 8 | 3060 |

plate shape. An injection nozzle for fuel is located in the center of the baffle plate and is surrounded by six oxidant injection holes. Here, $D_o$ is oxidant hole diameter and $D_f$ the fuel nozzle diameter. $L$ is the streamwise length of the computational domain. $L/D_f$ is 12.5 and $D_{tube}/D_f$ is 5.5 for the case A in Table 1. As illustrated in Table 1, the diameter ratio, $D_o/D_f$, is changed so that the oxidant to fuel velocity ratio $V_o/V_f$ is changed. In Fig. 2, $x$, $y$ and $z$ axes correspond to streamwise, transverse and spanwise directions, respectively for case A. The total grid number is set as $51 \times 55 \times 109$ through grid dependency test for all the three cases of Table 1. For the inlet boundary condition, the three dimensional, unsteady nature of turbulence is considered as superposing random perturbation on streamwise velocity component as follows:

$$u = U_{inlet}(1 + I\Phi), \tag{6}$$

here $\Phi$ is a probability function which returns real number randomly in the range of $-1 \leqslant \Phi \leqslant 1$ and $I$ is the fluctuation intensity. $U_{inlet}$ is the fuel or air inlet velocity described in Table 1 as $V_f$ or $V_o$. For the mixture fraction, $f = 1$ and $f = 0$ are applied to the fuel and air inlets, respectively. For outlet boundary conditions, convective boundary condition is used as follows:

$$\frac{\partial u_i}{\partial t} + U_{exit}\frac{\partial u_i}{\partial x_j} = 0, \tag{7}$$

where $U_{exit}$ is the mean velocity over the outflow boundary and $\partial f/\partial x = 0$ is adopted for a passive scalar. In the wall boundary condition, no-slip and non-permeable condition are adopted.

To determine calculation condition for the mass flow rate of fuel and oxidant, experimental results [7] are used as follows. Fig. 3 shows the blowout limit [7] of the flame experimentally obtained in a micro combustor with baffle plate B specified in Table 1. In case B, the mixing rate and flame stability are lower than those of other two cases. In the figure, $\dot{Q}_{oxidant}$ and $\dot{Q}_{fuel}$ mean the total volume flow rates of the oxidant and fuel which are entering into the combustor, respectively. The $\dot{Q}_{max}$ indicates the maximum volume flow rate of oxidant below which blowout of the flame does not occur and its value is $\dot{Q}_{max} = 8.0 \times 10^{-4}$ m$^3$/s. For the selected volume flow rate in Fig. 3, distinguished mixing pattern can be seen with each baffle plate as will be discussed later. Reynolds number based on the total gas flow rate and on the inner tube diameter of micro combustor, $D_{tube}$, is kept constant and $Re_{tube} = 3060$ and $D_{tube} = 2.2 \times 10^{-2}$ m for all the three cases. This means that

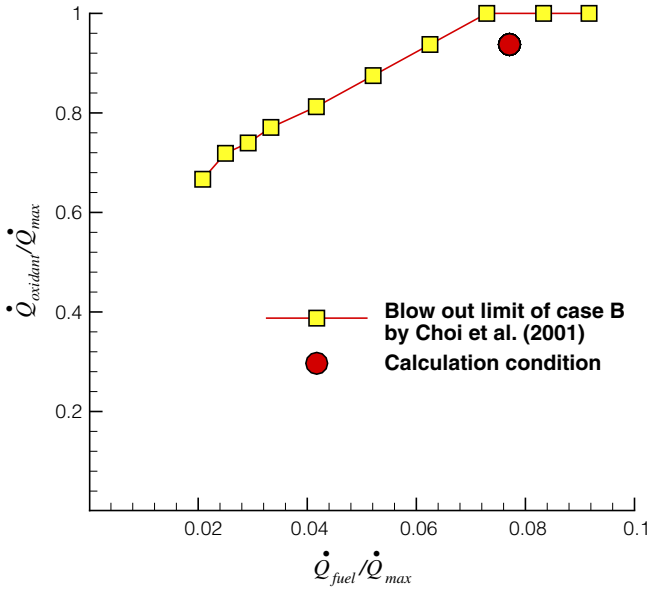


Fig. 3. Blowout limit of the flame in a micro can combustor in case B.

each of the fuel and oxidant flow rates is kept constant but their velocities are changed.

### 2.4. Capturing the vortices

In the present study, to detect the vortices negative $\Lambda_2$ is used to capture a vortical flow region as proposed by Jeong and Hussain [18] and Jeong et al. [19] and applied by Choi and Suzuki [20] in the LES study of turbulent heat transfer from a wavy wall. So, at every grid point and at every time step, calculation was made for finding a quantity $\Lambda_2$, the second largest one among the three eigenvalues of $-(1/\rho)(\partial^2 p/\partial x_i \partial x_j)$ or specially of its equivalent $S_{ik}S_{kj} + \Omega_{ik}\Omega_{kj}$. At each instant, attention was paid to the value of $\Lambda_2$ calculated at grid points over whole computational domain and negative $\Lambda_2$ region is regarded as vortical flow region.

## 3. Results and discussion

### 3.1. The characteristics of turbulent flow fields

First, the effect of baffle plate geometry is discussed in terms of time-averaged velocity field. Fig. 4 represents the vector map of time-averaged velocity and contour of time-averaged streamwise velocity in two different cross-sectional planes for the three different baffle plate cases. The upper cross-section shows the results in a plane slicing the middle of the space between the neighboring oxidant jets and the lower one shows the results in a plane slicing the center of a oxidant hole. In the figures, the magnitude of the velocity is non-dimensionalized by fuel inlet velocity $V_f$ of case A. In all the three cases, large flow recirculation regions appear near the combustor wall, namely both between fuel jet and wall and between air jet and wall.

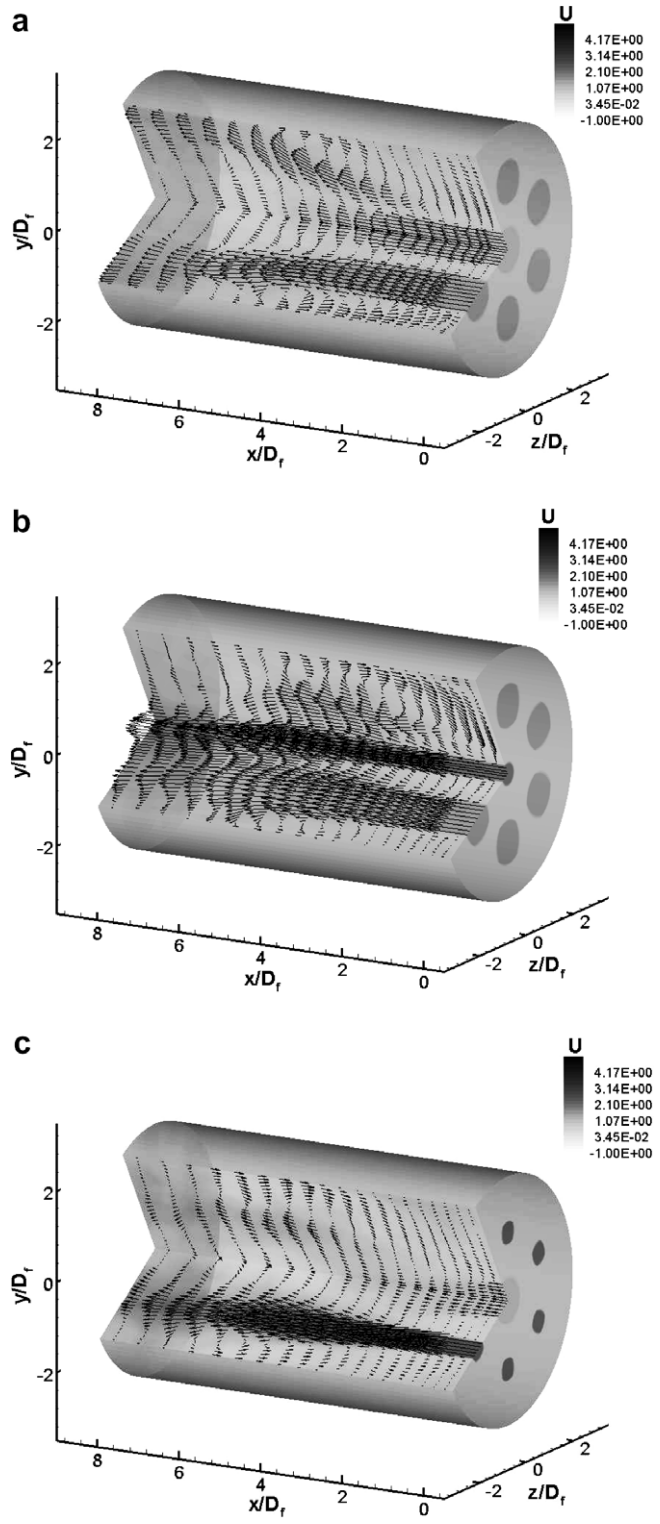


Fig. 4. Contour of streamwise velocity and velocity vector map in the two cross-sectional planes. (a) Case A; (b) Case B and (c) Case C.

These flow recirculation regions are called as near-wall flow recirculation regions in the following and the near-wall flow recirculation regions can be affected by the shape of baffle plate geometry like the one appearing downstream a backward facing step [21]. Peculiarity of the flow fields observed in two cases A and C is that, in addition to the near-wall flow recirculation regions, another flow recirculation region is formed downstream the fuel jet core region. This flow recirculation region is hereafter called as central flow recirculation region. This vortical flow can affect the mixing fields and actually is a key element of the enhanced mixing as will be discussed later. It may be worth to note that the central flow recirculation region is not found in case B. The central flow recirculation region ahead of the fuel jet originates from the lowering of fuel jet momentum due to the entrainment of fuel jet fluid into air jet.

Fig. 5 shows the iso-surfaces of instantaneous negative $\Lambda_2$ value captured at an instant in the half volume of the micro combustor for the baffle plates A, B and C. As can be seen in the figure, the generation of ring vortices is noticeable in the brim of oxidant jets and they develop

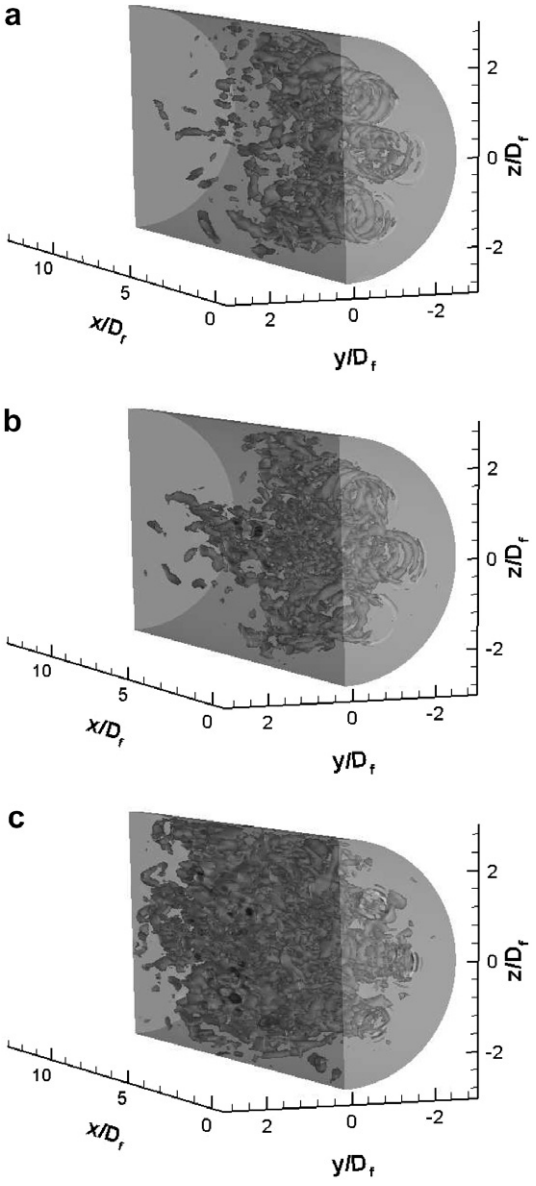


Fig. 5. Iso-surface of instantaneous negative $\Lambda_2$. (a) Case A; (b) Case B and (c) Case C.

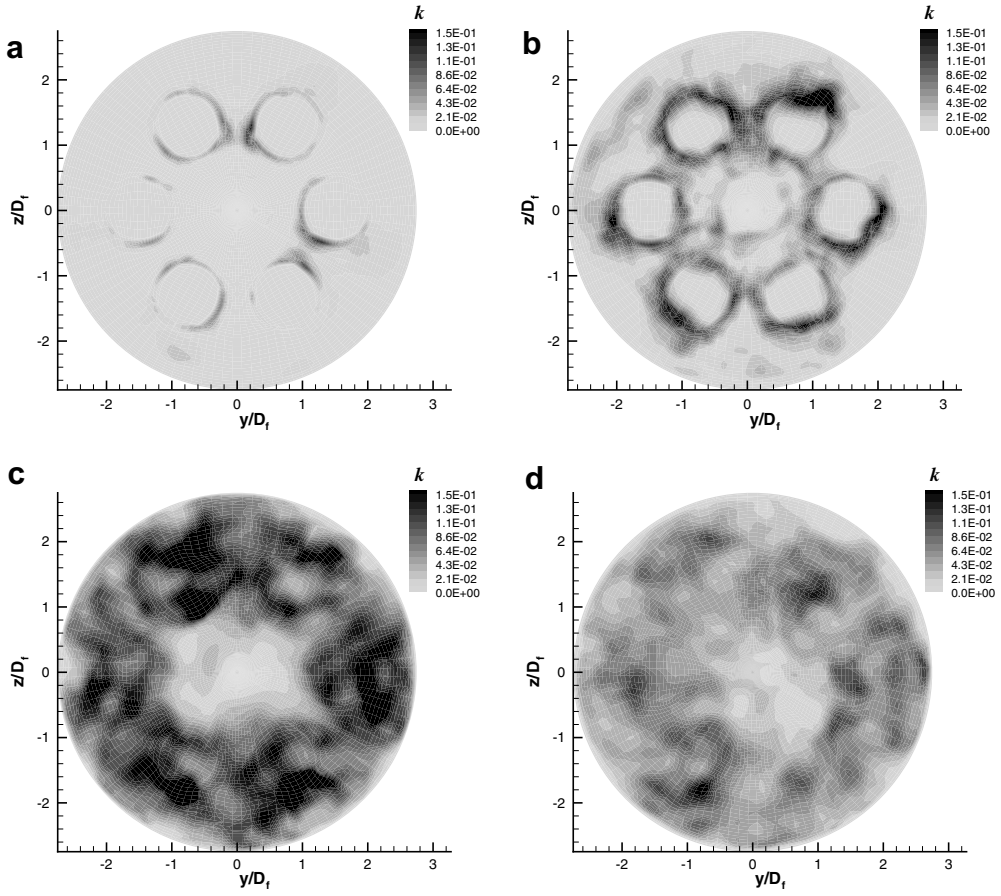


Fig. 6. Contour of turbulent kinetic energy at four different streamwise positions in case A. (a) $x/D_f = 1.0$; (b) $x/D_f = 2.5$; (c) $x/D_f = 5.5$ and (d) $x/D_f = 7.5$.

downstream and interact with each other, i.e. between neighboring vortices or between ring vortices and fuel jet. Note that this complex vortical region overlaps the central recirculation region. This makes the flow field downstream the baffle plate more vigorously turbulent and significantly enhances the scalar mixing there at such a low Reynolds number condition.

Fig. 6 shows the contours of turbulent kinetic energy $k = \frac{1}{2}(\overline{u_i' u_i'})$ in $(y, z)$ cross-sectional planes at different streamwise positions for case A. As observed in Fig. 6a, higher turbulent regions are limited at the edge of each oxidant jet and of ring shape at the first two locations downstream the baffle plate. These regions overlap the regions where the appearance of ring vortex is identified in Fig. 5a, which means that the shear layer caused by the vortices may affect the turbulent kinetic energy. This distribution pattern of turbulent kinetic energy is vaguely still observed at $x/D_f = 5.5$ in Fig. 6c. Mixing and dissipation of turbulence proceed toward downstream. Turbulent kinetic energy is now lowered and distributes almost uniformly in the cross-section at $x/D_f = 7.5$. This suggests that mixing of the scalar quantity is almost completed at this position. Fig. 7 compares the turbulent kinetic energy in the cross-section at $x/D_f = 2.5$ among the three cases with different baffle shapes. In case C, where air to fuel jet velocity ratio is the largest, ring vortices are most vigorously generated in the air jet shear layer and turbulent kinetic energy takes the largest value there among the three cases. From the above results, it is expected that the higher turbulent region affected by shear layer of the vortices caused by the oxidant jet makes the turbulent scalar mixing very efficient.

### 3.2. The characteristics of turbulent mixing fields

Fig. 8 shows the contours of time mean streamwise velocity and mixture fraction in the two cross-sectional planes. The contour of mixture fraction is expressed by color grade and streamwise velocity contour is drawn by a solid line for positive value and a dotted line for negative one. In all the three cases, the near-wall flow recirculation regions persistently appear between jets (fuel or oxidant) and combustor wall especially noticeable in the upstream half of the computational domain. However, the central flow recirculation region appears in the central region downstream the fuel jet only in the cases A and C. This central flow recirculation region produces rapid mixing of fuel and oxidant. So, the region where mean mixture fraction, $F$ takes a value larger than 0.5, is short in these cases compared with the case B. Furthermore, in case C,

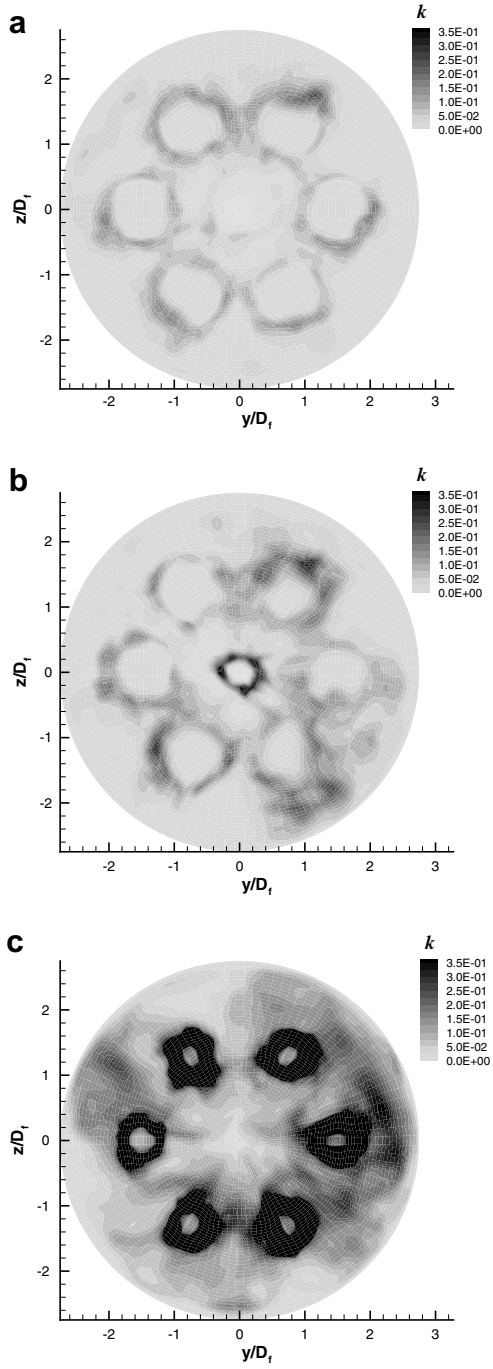


Fig. 7. Contour of turbulent kinetic energy at $x/D_f = 2.5$. (a) Case A; (b) Case B and (c) Case C.

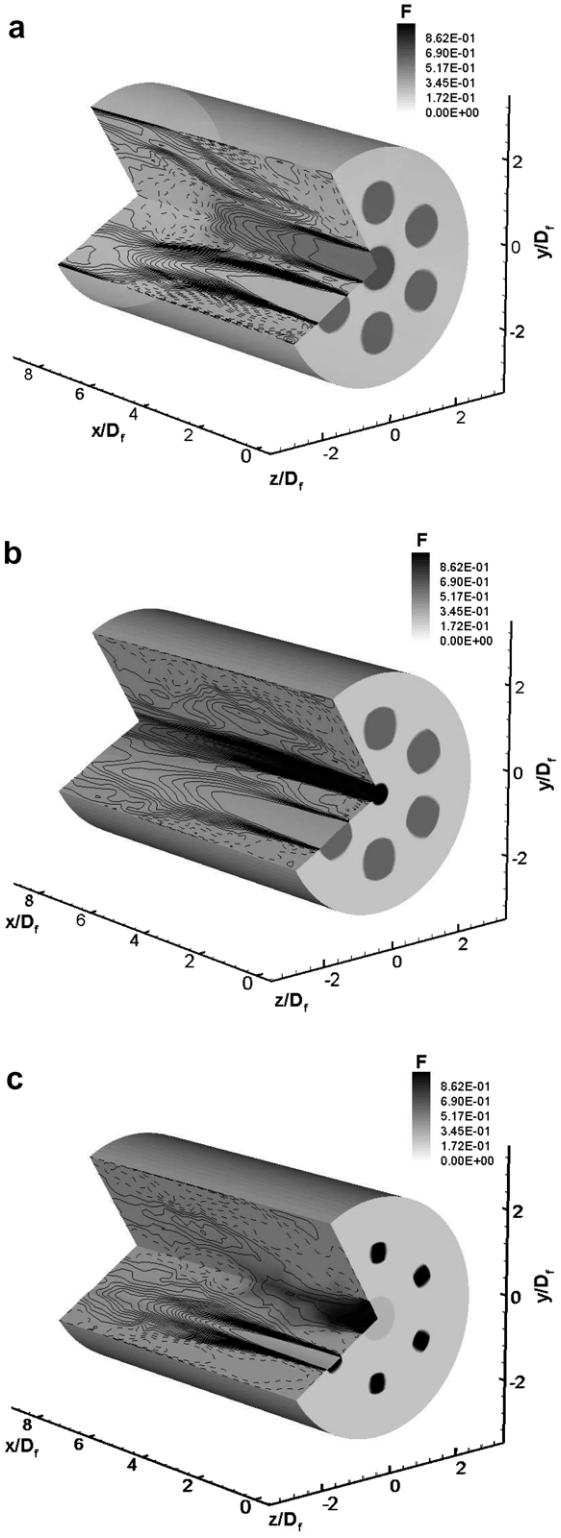


Fig. 8. Contours of steamwise velocity and mixture fraction. (a) Case A; (b) Case B and (c) Case C.

upstream edge of the central flow recirculation region formed downstream the fuel jet moves upstream resulting in the shortest high $F$ region or in the most effective mixing among the three cases.

Now, the characteristics of scalar mixing will be discussed in more detail. Fig. 9 shows the streamwise distribution of coefficient of variation, CV [22]. It represents the degree of non-uniformity of the spatial distribution of $F$ and is defined as follows:

$$\mathrm{CV} = \frac{1}{(F_i)_{\mathrm{cs}}}\sqrt{\frac{\sum_{i=1}^{n}[F_i - (F_i)_{\mathrm{cs}}]^2}{(n-1)}}, \tag{8}$$

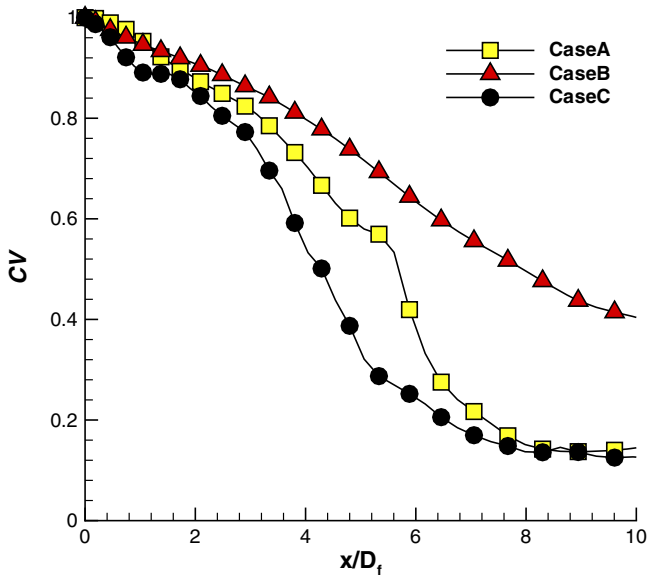


Fig. 9. Streamwise distribution of coefficient of variation.

where $F_i$ is the value of $F$ sampled at a grid point $i$ in a cross-section and $(F_i)_{cs}$ means the $(y,z)$ cross-sectional averaged value of $F_i$, therefore of $F$. So, CV is the standard deviation of mixture fraction divided by the spatial average of $F$ in a $(y,z)$ cross-sectional plane and it takes zero when $F$ distributes completely uniform in a cross-section. In case B, CV decreases along the streamwise direction with almost same slope over the entire region. In cases A and C, however, slope of CV curve changes noticeably around the central flow recirculation region and CV decreases more rapidly compared with case B. In case C, the decreasing rate of CV is the largest among the three cases. So, the case C shows the most effective scalar mixing or complete mixing within shorter streamwise length. Note that as discussed before, complex vortical region originated from the ring vortices overlaps the central flow recirculation region and helps the turbulent mixing as do the flow recirculation regions. In the following, this will be studied specifically paying attention to the turbulent mixing and their effects on consequent molecular mixing.

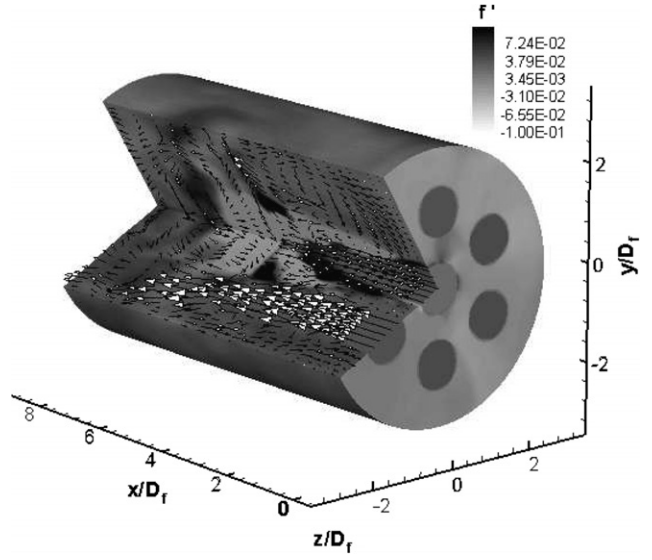


Fig. 10. Contours of instantaneous streamwise velocity and fluctuation of mixture fraction for case A.

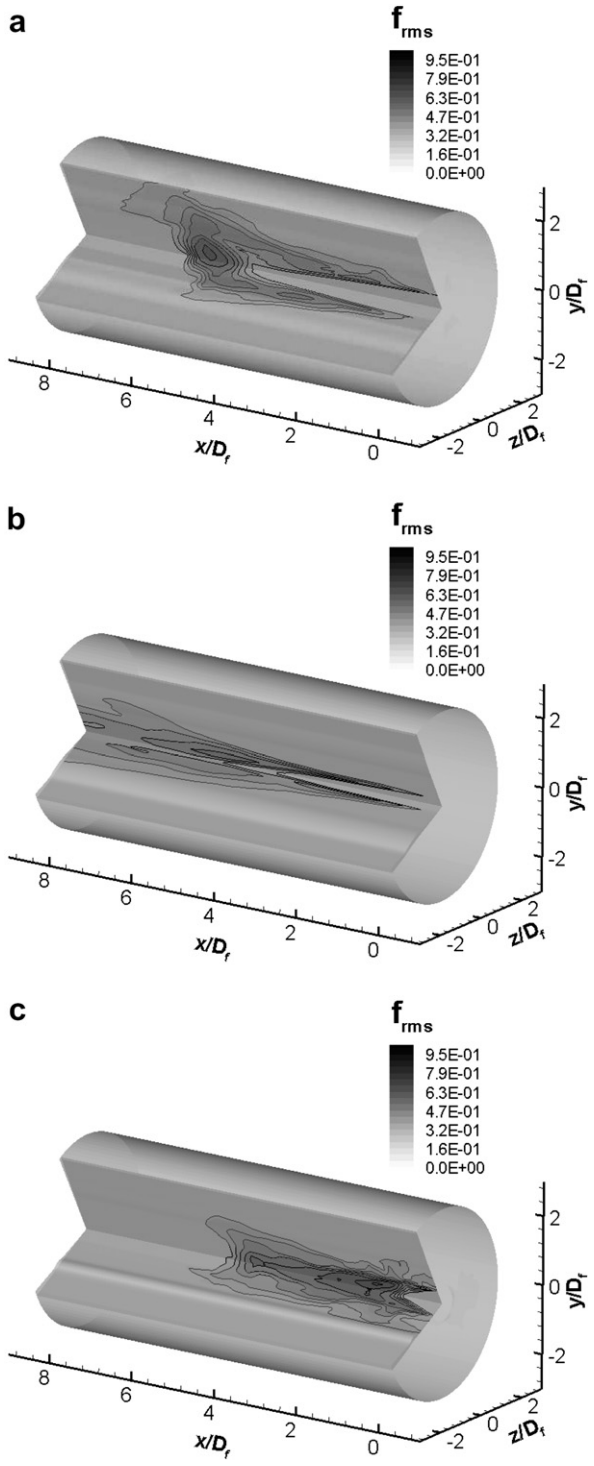


Fig. 11. Contours of $f_{rms}$ for the three different baffle plate cases. (a) Case A; (b) Case B and (c) Case C.

Fig. 10 displays the instantaneous velocity vector map and fluctuation of mixture fraction for the baffle plate A. Here, the fluctuation of the mixture fraction is defined as $f' \equiv f - F$ where $f$ and $F$ are the instantaneous and time mean values of mixture fraction, respectively. Contour of $f'$ is displayed by color grade. From the instantaneous velocity vector map, near the central flow recirculation region, the fluctuation of mixture fraction, $f'$, has high negative or positive magnitude. This suggests that active scalar mixing takes place as a result of the vigorous flow recirculation and fluctuation. This is more clearly recognized by seeing the fluctuation intensity of mixture fraction. In Fig. 11, the contours of $f_{\mathrm{rms}}$ are plotted and rms value of mixture fraction fluctuation is given as $f_{\mathrm{rms}} = \sqrt{\overline{(f-F)^2}}$. In case B, high $f_{\mathrm{rms}}$ region is located around the fuel jet and the magnitude of $f_{\mathrm{rms}}$ gradually decreases toward downstream. In cases A and C, on the other hand, maximum region of $f_{\mathrm{rms}}$ appears in the central region and after its maximum region, magnitude of $f_{\mathrm{rms}}$ drastically drops. Furthermore, the distance between fuel nozzle and the maximum location of $f_{\mathrm{rms}}$ becomes much shorter in case C than case A. Location and size of high $f_{\mathrm{rms}}$ region are close to the counterparts of central flow recirculation region. Note that in the upper section of cases A and C, high region of $f_{\mathrm{rms}}$ stems from the fuel jet flow and it reaches very close to the wall. This may the effect of the near-wall flow recirculation region. Along the streamwise direction, the decay of $f_{\mathrm{rms}}$ is steeper in magnitude in the order of the cases C, A and B. This implies that the progress of mixing will also be completed in small-scale in that order and this will be discussed in detail in the following.

To scrutinize small-scale mixing, dissipation rate of the scalar variance is defined as follows:

$$\epsilon_{\mathrm{f}} = D\left(\frac{\partial f'}{\partial x_j}\right)^2 = \frac{v}{Sc}\left(\frac{\partial f'}{\partial x_j}\right)^2. \tag{9}$$

This dissipation rate of scalar variance can be understood as decaying rate of scalar fluctuation. Larger value of dissipation rate of scalar variance suggests more efficient stirring at small-scales. So, dissipation rate of scalar variance, $\epsilon_{\mathrm{f}}$, can be considered as corresponding to the molecular mixing rate as it is discussed by Dowling [23] and Yeung and Xu [24]. Furthermore, when combustion occurs in fast chemistry limit, chemical products are directly proportional to $\epsilon_{\mathrm{f}}$ [25–27]. Fig. 12 represents instantaneous contours of dissipation rate of scalar variance, $\epsilon_{\mathrm{f}}$, and streamwise velocity at two different cross-sectional planes. In all the three cases, local maxima of the scalar dissipation is located at the edge of the fuel jet flow along the streamwise direction. The length of the local maxima decreases in the order of the cases B to A, and C. Note that in cases A and C, the magnitude of $\epsilon_{\mathrm{f}}$ drastically drops upstream of the central flow recirculation region. So, it can be expected that the central flow recirculation region helps the molecular mixing as well as turbulent mixing and this can be more clearly seen by the spatial average of time mean value of $\epsilon_{\mathrm{f}}$ over the $(y,z)$ cross-section, $\bar{\epsilon}_{\mathrm{f}}$, plotted in Fig. 13.

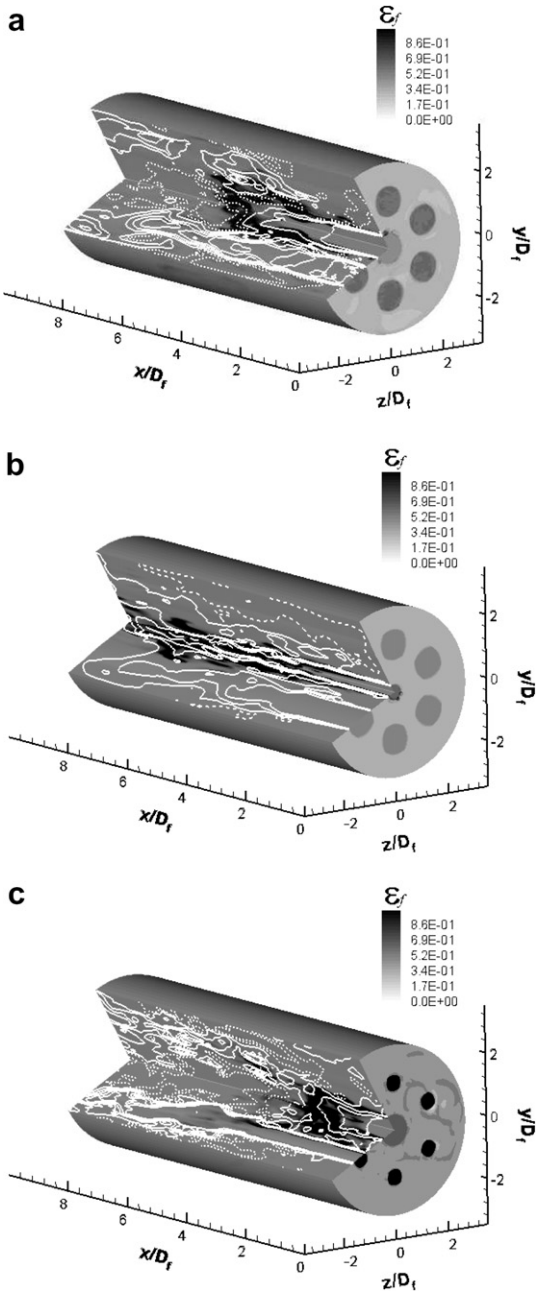


Fig. 12. Contours of instantaneous dissipation rate of scalar variance. (a) Case A; (b) Case B and (c) Case C.

In Fig. 13, it is observed that $\bar{\epsilon}_{\mathrm{f}}$ shows the most rapid increase and drop in the streamwise direction in case C and the slowest change in the case B. As discussed in Fig. 12, in cases A and C, the peak of $\bar{\epsilon}_{\mathrm{f}}$ appears at the brim of fuel jet and upstream the central flow recirculation region and the value of $\bar{\epsilon}_{\mathrm{f}}$ becomes zero near the end of the central recirculation region. This implies that high shear flow at the edge of the ring vortices and the central flow recirculation region play an important role for molecular mixing in cases A and C.

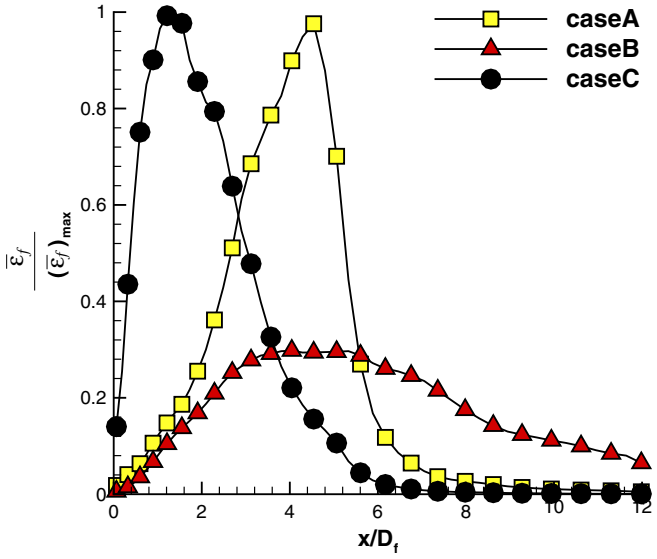


Fig. 13. Streamwise distribution of mean dissipation rate of scalar variance.

## 4. Concluding remarks

In the present study, turbulent mixing of passive scalar of multiple jet flows in a micro can combustor is investigated by means of Large Eddy Simulation (LES). The micro can combustor is characterized by a baffle plate having oxidizer holes and fuel nozzle and study was made in the three cases of different baffle plate configurations. The baffle plate is mounted to enhance the slow scalar mixing in the low Reynolds number condition of the micro combustor and to hold the flame stable. In this study, mixing is found to be greatly affected by the near-wall flow recirculation regions formed between jets and wall and the central flow recirculation region formed downstream the fuel jet flow. Especially, appearance of the central flow recirculation region plays an important role to enhance the turbulent mixing between fuel and oxidant fluids transporting the fuel into the oxidant flow or engulfing the oxidant flow into the fuel jet. As a result, in cases with the baffle plates A and C, central flow recirculation region is generated and turbulent mixing proceeds more effectively than in the case with the baffle plate B where no central flow recirculation region appears. In case C, air jet velocity is high and ring vortices appear most noticeably, intermingling with each other and develop most effectively into turbulent vortices. Also, this high momentum of air jet flow brings about the upstream movement of the central flow recirculation region and results in the completion of turbulent mixing within a shorter distance from the baffle plate. In other words, the high shear flow with ring vortices overlaps the central flow recirculation region and these two particular flow patterns much accelerate the turbulent mixing. The dissipation rate of scalar variance is also found the largest magnitude and has the fastest increase and drop in case C. Therefore, molecular-scale mixing also proceeds effectively with the baffle plate C. Consequently, short flame length is expected to be achieved in this case or in the case where air jet velocity is high. It notes that if the sophisticated model is used for SGS scalar flux the turbulent scalar field might be influenced. However, as discussed in Pitsch [13] its effect can be minimized by careful selection of turbulent Shcmidt number. So, in the present study an eddy diffusivity model for SGS scalar flux is adopted discreetly and this might be enough to reach the goal of the present study.

## References

[1] C.F. Mcdonald, Low cost compact primary surface recuperator concept for microturbines, Appl. Therm. Eng. 20 (2000) 471–497.
[2] R.J. Kee, H. Zhu, D.G. Goodwin, Solid-oxide fuel cells with hydrocarbon fuels, Proc. Combust. Inst. 30 (2005) 2379–2404.
[3] K. Suzuki, K. Teshima, J.H. Kim, Key note paper: solid oxide fuel cell and micro gas turbine hybrid cycle for a distributed energy generation system, in: Proceedings of the 4th JSME-KSME Thermal Engineering Conference, 13, 2000, pp. 1–8.
[4] A.F. Massardo, F. Lubelli, Internal reforming solid oxide fuel cell-gas turbine combined cycles(IRSOFCGT): Part A – cell model and cycle thermodynamics analysis, Trans. ASME J. Eng. Gas Turb. Power 122 (2000) 27–35.
[5] S. Kimijima, N. Kasagi, Performance evaluation of gas turbine-fuel cell hybrid micro generation system, Proc. ASME Turbo Expo, 2002, GT-2002-30111.
[6] A.C. Fernandez-Pello, Micropower generation using combustion: issues and approaches, Proc. Combust. Inst. 29 (2002) 883–899.
[7] H.S. Choi, K. Nakabe, K. Suzuki, Y. Katsumoto, An experimental investigation of mixing and combustion characteristics on the can-type micro combustor with a multi-jet baffle plate, Fluid Mech. Appl. 70 (2001) 367–375.
[8] H.S. Choi, T.S. Park, K. Suzuki, LES of turbulent flow and mixing in a micro can combustor, in: Proceedings of the 4th International Symposium Turbulence and Shear Flow Phenomena, 2, 2005, pp. 389–394.
[9] H.S. Choi, T.S. Park, K. Suzuki, Numerical analysis on the mixing of a passive scalar in the turbulent flow of a small combustor by using large eddy simulation, J. Comput. Fluid Eng. (Korean) 11 (2006) 67–74.
[10] V. Zhdanov, N. Kornev, E. Hassel, A. Chorny, Mixing of confined coaxial flows, Int. J. Heat Mass Transfer 49 (2006) 3942–3956.
[11] P.L. Woodfield, K. Nakabe, K. Suzuki, Numerical study for enhancement of laminar flow mixing using multiple confined jets in a micro-can combustor, Int. J. Heat Mass Transfer 46 (2003) 2655–2663.
[12] D.K. Lilly, A proposed modification of the Germano subgrid-scale closure model, Phys. Fluids 4 (1992) 633–635.
[13] H. Pitsch, H. Steiner, Large eddy simulation of a turbulent piloted methane/air diffusion flame (Sandia flame D), Phys. Fluids 12 (2000) 2541–2554.
[14] R.I. Issa, Solution of the implicitly discretized fluid flow equations by operating-splitting, J. Comput. Phys. 62 (1986) 40–65.
[15] T.S. Park, Effect of time-integration method in a large eddy simulation using PISO algorithm: Part I – flow field, Numer. Heat Transfer Part A 50 (2006) 229–245.
[16] T.S. Park, Effect of time-integration method in a large eddy simulation using PISO algorithm: Part II – thermal field, Numer. Heat Transfer Part A 50 (2006) 247–262.
[17] S.K. Lele, Compact finite difference schemes with spectral-like resolution, J. Comput. Phys. 103 (1992) 16–42.
[18] J. Jeong, F. Hussain, On the identification of a vortex, J. Fluid Mech. 285 (1995) 69–94.

[19] J. Jeong, F. Hussain, W. Schoppa, J. Kim, Coherent structures near the wall in a turbulent channel flow, J. Fluid Mech. 332 (1997) 184–214.
[20] H.S. Choi, K. Suzuki, Large eddy simulation of turbulent flow and heat transfer in a channel with one wavy wall, Int. J. Heat Fluid Flow 26 (2005) 681–694.
[21] H. Le, P. Moin, J. Kim, Direct numerical simulation of turbulent flow over a backward-facing step, J. Fluid Mech. 330 (1997) 349–374.
[22] J. Aubin, D.F. Fletcher, J. Bertrand, C. Xuereb, Characteristics of the mixing quality in micromixers, Chem. Eng. Technol. 26 (2003) 1262–1270.
[23] Dowling, R. David, The estimated scalar dissipation rate in gas-phase turbulent jets, Phys. Fluids 16 (1991) 93–103.
[24] P.K. Yeung, Jia Xu, Effects of rotation on turbulent mixing: nonpremixed passive scalars, Phys. Fluids 16 (2004) 93–103.
[25] R.W. Bilger, Some aspects of scalar dissipation, Turb. Flow Combust. 72 (2004) 93–114.
[26] D.A. Donzis, K.R. Sreenivasan, P.K. Yeung, Scalar dissipation rate and dissipative anomaly in isotropic turbulence, J. Fluid Mech. 32 (2005) 199–216.
[27] K.R. Sreenivasan, Possible effects of small-scale intermittency in turbulent reacting flows, Turb. Flow Combust. 72 (2004) 115–131.